Neurobiology of Disease 121 (2019) 1–16

Contents lists available at ScienceDirect

Neurobiology of Disease

journal homepage: www.elsevier.com/locate/ynbdi

Accelerated accumulation of retinal α-synuclein (pSer129) and tau, neuroinflammation, and autophagic dysregulation in a seeded mouse model of Parkinson's disease

Najiba Mammadova[a,b,c], Corey M. Summers[b,d,1], Robyn D. Kokemuller[c,e,f,1], Qing He[g], Shaowei Ding[h], Thierry Baron[i], Chenxu Yu[g], Rudy J. Valentine[b,d], Donald S. Sakaguchi[a,c], Anumantha G. Kanthasamy[b,c,f], Justin J. Greenlee[e], M. Heather West Greenlee[b,c,f,*]

[a] Department of Genetics, Development, and Cell Biology, Iowa State University, Ames, IA, United States
[b] Immunobiology Graduate Program, Iowa State University, United States
[c] Neuroscience Graduate Program, Iowa State University, United States
[d] Department of Kinesiology, Iowa State University, United States
[e] Virus and Prion Research Unit, National Animal Disease Center, USDA, Agricultural Research Service, Ames, IA, United States
[f] Department of Biomedical Sciences, Iowa State University College of Veterinary Medicine, Ames, IA, United States
[g] Department of Agriculture and Biosystems Engineering, Iowa State University, Ames, IA, United States
[h] Department of Mechanical Engineering, Iowa State University, Ames, IA, United States
[i] Anses, Laboratoire de Lyon, Unité Maladies Neurodégénératives, Lyon, France

ARTICLE INFO

Keywords:
Retina in Parkinson's Disease
Photoreceptor cell loss
Tau in retina
Microglial activation in retina
Müller glial activation
Misfolded α-synuclein
Human A53T mutated α-synuclein
Autophagy in PD retina
Raman Spectroscopy

ABSTRACT

Parkinson's disease (PD) is a neurodegenerative disorder characterized by accumulation of misfolded α-synuclein within the central nervous system (CNS). Visual problems in PD patients are common, although retinal pathology associated with PD is not well understood. The purpose of this study was to investigate retinal pathology in a transgenic mouse model (TgM83) expressing the human A53T α-synuclein mutation and assess the effect of α-synuclein "seeding" on the development of retinal pathology. Two-month-old TgM83 mice were intracerebrally inoculated with brain homogenate from old (12–18 months) TgM83 mice. Retinas were then analyzed at 5 months of age. We analyzed retinas from 5-month-old and 8-month-old uninoculated healthy TgM83 mice, and old (12–18 months) mice that were euthanized following the development of clinical signs. Retinas of B6C3H mice (genetic background of the TgM83 mouse) served as control. We used immunohistochemistry and western blot analysis to detect accumulation of α-synuclein, pTau^{Thr231}, inflammation, changes in macroautophagy, and cell death. Raman spectroscopy was used to test the potential to differentiate between retinal tissues of healthy mice and diseased mice. This work demonstrates retinal changes associated with the A53T mutation. Retinas of non-inoculated TgM83 mice had accumulation of α-synuclein, "pre-tangle" tau, activation of retinal glial cells, and photoreceptor cell loss by 8 months of age. The development of these changes is accelerated by inoculation with brain homogenate from clinically ill TgM83 mice. Compared to non-inoculated 5-month-old TgM83 mice, retinas of inoculated 5-month-old mice had increased accumulation of α-synuclein (pSer129) and pTau^{Thr231} proteins, upregulated microglial activation, and dysregulated macroautophagy. Raman spectroscopic analysis was able to discriminate between healthy and diseased mice. This study describes retinal pathology resulting from the A53T mutation. We show that seeding with brain homogenates from old TgM83 mice accelerates retinal pathology. We demonstrate that Raman spectroscopy can be used to accurately identify a diseased retina based on its biochemical profile, and that α-synuclein accumulation may contribute to accumulation of pTau^{Thr231} proteins, neuroinflammation, metabolic dysregulation, and photoreceptor cell death. Our work provides insight into retinal changes associated with Parkinson's disease, and may contribute to a better understanding of visual symptoms experienced by patients.

* Corresponding author at: College of Veterinary Medicine, 2008 Vet Med, 1800 Christensen Drive, Ames, IA 50010, United States.
E-mail addresses: najibam@iastate.edu (N. Mammadova), summers@iastate.edu (C.M. Summers), robynk13@iastate.edu (R.D. Kokemuller), qinghe@iastate.edu (Q. He), swding@iastate.edu (S. Ding), thierry.baron@anses.fr (T. Baron), chenxuyu@iastate.edu (C. Yu), rvalenti@iastate.edu (R.J. Valentine), dssakagu@iastate.edu (D.S. Sakaguchi), akanthas@iastate.edu (A.G. Kanthasamy), Justin.Greenlee@ars.usda.gov (J.J. Greenlee), mheather@iastate.edu (M. Heather West Greenlee).

[1] Authors have made equal contributions to the manuscript, with names listed alphabetically.

https://doi.org/10.1016/j.nbd.2018.09.013
Received 3 July 2018; Received in revised form 5 September 2018; Accepted 11 September 2018
Available online 12 September 2018

List of abbreviations

PD	Parkinson's Disease
CNS	Central nervous system
SNpc	substantia nigra pars compacta
TH	Tyrosine hydroxylase
MSA	multiple system atrophy
PSP	progressive supranuclear palsy
AD	Alzheimer's Disease
CMA	chaperone-mediated autophagy
TSEs	transmissible spongiform encephalopathies
GCL	ganglion cell layer
INL	inner nuclear layer
IPL	inner plexiform layer
OPL	outer plexiform layer
ONL	outer nuclear layer

1. Introduction

Parkinson's disease (PD) is a neurodegenerative disorder characterized by two key disease processes: progressive degeneration of dopaminergic neurons of the substantia nigra pars compacta (SNpc) in the midbrain that leads to deficits in voluntary movement, and the accumulation of intraneuronal Lewy-bodies, containing misfolded α-synuclein (Recasens and Dehay 2014). Prominent non-motor phenomena, specifically visual disturbances, are a considerable cause of morbidity in Parkinson's disease (Archibald et al. 2009; Armstrong 2011). There is evidence of visual dysfunction at several levels of the visual pathway in patients with PD, including morphological and electrophysiological indication of disruption of retinal structure and function (Armstrong 2011; Bodis-Wollner 2013; Ridder et al. 2017). However, the direct effect of misfolded α-synuclein on the retina is not well understood, and molecular biomarkers of PD progression in the retina are lacking.

Here, we use the TgM83 mouse model to investigate retinal pathology due to a human α-synuclein (A53T) gene mutation. We also use this model to study the effect of α-synuclein seeding in the brain, on development of pathology in the retina. Often referred to as “prion-like propagation”, the transport of misfolded proteins from one central nervous system structure (CNS) seeds protein misfolding and propagation in another (Angot et al. 2010; Greenlee et al. 2016; Luk et al. 2012a; Mougenot et al. 2012; Watts et al. 2013; Woerman et al. 2017). This is consistent with the Braak staging of Parkinson's disease, which describes a progressive and non-random process with specific neuronal types giving rise to the development of Lewy pathology in a specific pattern (i.e. caudo-rostral progression of disease from the lower brainstem, followed by the midbrain, forebrain, and cerebral cortex) and as disease progresses, lesion severity in vulnerable brain regions increases (Braak et al. 2003). A growing body of in vitro and in vivo evidence describes the ability of pathological α-synuclein to spread transcellularly and induce aggregation by templating protein misfolding (Angot et al. 2010; Katorcha et al. 2017; Luk et al. 2012a; Luk et al. 2012b; Mougenot et al. 2012; Woerman et al. 2017). An in vivo study shows that seeding with an inoculum derived from the brain of clinically ill mice, results in acceleration of α-synuclein-associated disease and shortening of survival time (Mougenot et al. 2012). Disease acceleration is associated with an insoluble form of α-synuclein phosphorylated on serine 129 (Mougenot et al. 2012). Among several existing post-translational modifications to α-synuclein known to occur in PD, phosphorylation at Ser129 (herein referred to as pSer129), has been reported to enhance α-synuclein toxicity both in vitro and in vivo (Chen et al. 2009; Fujiwara et al. 2002; Smith et al. 2005). Although α-synuclein is not an infectious agent, studies attribute the enhanced toxicity of pSer129 to increased formation and self-propagation of α-synuclein aggregates (Angot et al. 2010). In this study, we use a mouse model of α-synuclein seeding to study the effect of α-synuclein spreading in the CNS, specifically on development and progression of retinal pathology. Herein, we report the time course of specific retinal changes associated with the A53T mutation, including: accumulation of pSer129 and ‘pre-tangle tau protein in the retina, dysregulation of macroautophagy in response to the increase in misfolded proteins, and loss of photoreceptors. We demonstrate accelerated development of pathologic biomarkers in mice inoculated with brain homogenate from clinically ill TgM83 mice.

We also explored the use of Raman spectroscopy to identify disease-specific molecular signatures in retinal tissues from α-synuclein A53T mutant mice. Raman spectroscopy is a sensitive and nondestructive technique that provides rapid biochemical characterization of tissues for diverse applications (Wang et al. 2011). The Raman effect occurs when an incident monochromatic light, emitted by a laser, scatters when it passes through a substance. The scattered light is inelastic, meaning it contains additional frequencies that are different than that of the incident frequency. These frequencies (i.e. emitted photons) are captured by a Raman spectrophotometer, and the resulting spectrum reveals fingerprint regions specific to molecules' chemical bonds and configurations. Raman spectra collected from samples are used to train and test a classifier to accurately discriminate between diseased and healthy tissues according to changes in their molecular structure. Several neurodegenerative diseases result from misfolding and accumulation of specific proteins (e.g. α-synuclein and tau in Parkinson's disease, tau and beta-amyloid in Alzheimer's disease, and prion proteins in transmissible spongiform encephalopathies) that change the chemical composition of tissues. Here, Raman spectroscopy was used to differentiate between the biochemical fingerprints of retinal tissues from healthy mice and mice with the α-synuclein A53T mutation. The classifier was able to discriminate between retinal tissues of control, healthy, and diseased mice with high accuracy, even between samples that appeared histologically similar.

To the best of our knowledge, this report is the first to demonstrate retinal pathology resulting from the A53T mutation, and that seeding with brain homogenate from clinically ill mice accelerates retinal pathology. This work implies a direct effect of α-synuclein toxicity on the retina, causing chronic neuroinflammation, metabolic dysregulation and cell death. Additionally, this study describes the use of Raman spectroscopic analysis for the differentiation of control retinas and those affected by α-synuclein associated pathology, with high specificity. Here, we describe an in vivo model that provides insight into how Parkinson's disease affects the retina, and how α-synuclein related changes may contribute to visual disturbances experienced by patients.

2. Methods

2.1. Animals

Retinal tissues were provided by Thierry Baron (Anses, Laboratoire de Lyon, Unité Maladies Neurodégénératives, Lyon, France). Briefly, 2-month-old homozygous TgM83 mice were subjected to intracerebral ventricular inoculation (ICV) with 20 µL of 1% (wt/vol in glucose 5%) brain homogenates obtained from half of the brain of clinically ill TgM83 mice (12–18 months), and euthanized three months after IC inoculation, corresponding to a pre-clinical stage (Mougenot et al. 2012). Clinically-ill TgM83 mice were euthanized following the development of motor clinical signs of disease, in this case paralysis of the hind limbs. Care and housing of mice, as well as ethical approval is described as per Mougenot et al., 2011. Eye globes were postfixed in Bouin's fixative for 24 h, embedded in paraffin, and sectioned sagitally at 4-µm onto superfrost plus glass slides. We analyzed retinas of homozygous TgM83 mice at 5, 8 (clinical illness), and 12–18 (clinical illness) months of age; inoculated TgM83 mice at 5 months of age; and

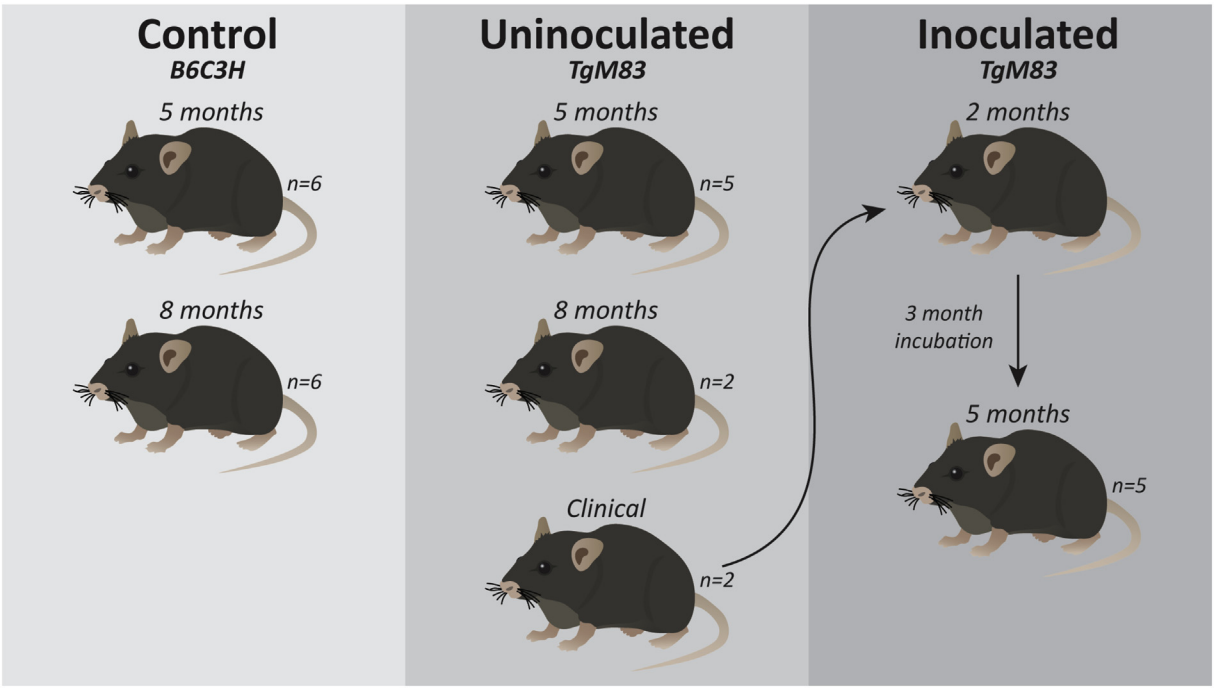

Fig. 1. Experimental Design. Retinas of transgenic mice (TgM83) at 5, 8, and 12–18 months of age, and age-matched controls (B6C3H) were analyzed using immunohistochemistry and western blotting. Additionally, retinas of 2-month-old TgM83 mice were inoculated with brain homogenate from clinically ill (12–18-month-old) TgM83 mice, and retinal tissues were analyzed 3 months later.

B6C3H mice (genetic background of the TgM83 mouse model) at 5 and 8 months of age (Fig. 1).

2.2. Immunohistochemistry

Paraffin-embedded sections (4 μm) of the retina were rehydrated using xylene, followed by a decreasing ethanol concentration gradient (100%, 90% 70%), and a final wash with diH_2O. Heat-mediated antigen retrieval was performed using EDTA buffer (10 mM Trizma Base, 1 mM EDTA solution, 0.05% Tween 20, pH 9.0), or Citrate buffer (ScyTek Laboratories, Logan, UT) in an autoclave for 30 min. Tissues were incubated with Background Buster (Innovex Biosciences Inc., Richmond, CA) for 2 h. Primary antibodies against α-synuclein (1:1000, BD Biosciences, San Jose, CA, 610786), α-synuclein p129S (1:500; Abcam, Cambridge, MA, ab51253), tyrosine hydroxylase (1:50, Santa Cruz Biotechnology, Dallas, TX), glial fibrillary acidic protein (GFAP; 1:500; Dako, Carpinteria, CA), CD11b (1:500; Abcam), CD68 (1:100; Abnova, Taiwan), PHF-Tau Clone AT-180 (1:100; Thermo Fisher Scientific, Inc., Rockford, IL), calbindin (1:2000, Swant, Inc., Switzerland), LC3 (1:1000, Cell Signaling, Danvers, Massachusetts), or caspase-3 (1:50, Santa Cruz Biotechnology) were diluted in blocking solution containing 0.1% bovine serum albumin (BSA; Sigma-Aldrich, St. Louis, MO), 0.05% Triton X-100 (Thermo Fisher Scientific, Inc., Rockford, IL) and 5% normal serum (Jackson ImmunoResearch, West Grove, PA) in Tris-Buffered saline (TBS), and incubated for 48 h at room temperature. Tissues were washed with TBS-T (6 × 5 min) and incubated with a secondary antibody cocktail, including Cy™3 and/or Alexa Fluor 488–conjugated AffiniPure secondary antibodies (1:250; Jackson ImmunoResearch) and 40,6-diamidino-2phenylindole, dilactate (DAPI, 4 μg/mL; Sigma-Aldrich) for 1.5 h. Following another wash, slides were mounted with Vectashield antifade mounting medium (Vector Laboratories Inc., Burlingame, CA). Immunoreactivity for α-synuclein, α-synuclein p129S, tyrosine hydroxylase, and Caspase-3 was developed using Envision þ Dual Link System-horseradish peroxidase (Dako, Carpinteria, CA) with diaminobenzidine (Vector Labs, Peterborough, UK), and slides were counterstained with hematoxylin. Negative controls were processed in parallel by omission of the primary and/or secondary antibody.

2.3. Fluorescent microscopy and statistical analysis

Fluorescence and confocal images were taken at 20× and 60×, using a Nikon A1R+ Resonant Scanning Confocal System with a Ti-E inverted microscope and laser lines 405, 488, 561 and 640 nm (Nikon Instruments Inc., Melville, New York). Micrographs were created using a commercial photo-editing system (Adobe Photoshop and Adobe Illustrator [CC]; Adobe Systems). For quantification of GFAP, CD11b, AT-180, and CD68 immunoreactivity, the percentage of the total image area thresholded (outer limiting membrane to inner limiting membrane of the retina) was analyzed using ImageJ (Rasband, W.S., ImageJ 1.49 V, U. S. National Institutes of Health, Bethesda, Maryland). Quantified histological, and western blot data from three separate replicates was analyzed using a two-way ANOVA, with a Tukey's multiple comparisons test (post-hock). Thickness of the outer nuclear layer (ONL) was measured by counting of cell bodies spanning the layer. For each mouse, the central retina, near the optic disc, within a cross section was used for analysis. Retinal thickness was analyzed using an unpaired *t*-test. Prism 6 for Windows (Graph Pad Software) was used for statistical analysis.

2.4. Protein extraction from paraffin embedded tissues for western blot analysis

Bouin's fixed paraffin-embedded sections (100 μm total, 10 × 10 μm sections) of the retina were collected into 1.5 mL microcentrifuge tubes. Sections were deparaffinized and rehydrated using xylene, followed by a decreasing ethanol concentration gradient (100%, 95% 70%). Then, 100 μL of lysis buffer containing protease and phosphatase inhibitor cocktail was added to each sample, and samples were incubated on ice for 5 min. Samples were then incubated at 100 °C for 20 min, then again at 80 °C for 20 min using a thermomixer with agitation (750 rpm). Samples were then centrifuged for 15 min (14,000 g at 4 °C).

Supernatant was collected, and samples were kept overnight at −20 °C. Tissues containing equal amounts of protein were separated on 4–20% SDS-polyacrylamide gels. After separation, proteins were transferred to polyvinylidene difluoride (PVDF) membranes, and non-specific binding sites were blocked by treating with 5% non-fat dry milk in 0.5% TBS-T for 1 h. The membranes were then incubated with primary antibodies directed against α-synuclein (1:5000, BD Biosciences, San Jose, CA), α-synuclein p129S (1:1000; Abcam, Cambridge, MA), pAMPK^{T172} (1:1000, Cell Signaling, Danvers, Massachusetts), AMPK (1:1000, Cell Signaling), pULK1^{S757} (1:1000, Cell Signaling), ULK1 (1:1000, Cell Signaling), and LC3 (1:5000, Cell Signaling) overnight at 4 °C. The primary antibody treatments were followed by treatment with HRP-linked, anti-rabbit or anti-mouse secondary antibody (1:5000, Cell Signaling) for 1 h at room temperature. Western blot images were captured with the ChemiDoc™ XRS Imaging System (Bio-Rad), and images were analyzed using Image Lab™ 6.0 Software (Bio-Rad). All groups are normalized to 5-month-old B6C3H mice (genetic background of the TgM83 mouse model), providing a representative of a fold-change from the control, therefore y-axis units are arbitrary.

2.5. Raman spectroscopy

Paraffin-embedded sections (4 μm) of the retina were placed on gold-aluminum coated microscope slides. Raman measurements were performed using a DXR dispersive Raman microscope (Thermo Scientific, Inc., Madison, Wisconsin) with a 532 nm, 14 mW excitation laser with 50 μm pinhole at ambient temperature and collected with a 20s exposure time from 110 to 3527 cm^{-1} at a resolution of 1 cm^{-1}. Retinal ganglion cells were resolved with a 60× objective. Twenty spectra were collected from twenty different retinal ganglion cells at different locations and an average spectrum was then calculated for that cell to be used as one RGC spectrum in subsequent analysis (20 spectra from each retinal section, for a total of 400 spectra from each group). Raman peaks that exhibited the most significant changes between control and diseased tissue samples were identified. All spectra were baseline corrected, smoothed, and normalized to reduce baseline variability and background noise at the region between 110 and 3527 cm^{-1}, using an iterative correction algorithm (Wang et al. 2011) coded with R. After preprocessing, a principal component analysis (PCA) was used to reduce dimensionality. Multi-class classification was generated using a support vector machine (SVM) (Gunn 1998). Cross-validation was applied by randomly choosing 75% of the spectral data to build the classification model, using the remaining 25% of the spectra to test and validate the classifier. Average classification accuracy was calculated from 10 random replications of the discriminant process.

3. Results

3.1. Retinas of TgM83 mice exhibit α-synuclein accumulation

In Parkinson's disease, α-synuclein aggregates are highly enriched in α-synuclein that has been phosphorylated at serine 129 (pSer129), which has been reported to enhance the tendency of α-synuclein to aggregate and disrupt normal function in vitro and in vivo (Walker et al. 2013; Wang et al. 2012). To investigate whether α-synuclein pSer129 is present in retinas of transgenic mice, we performed immunohistochemistry and western blot analysis. In addition to probing for a specific pathogenic form of α-synuclein, we used immunohistochemistry and western blot analysis to determine levels and pattern of total α-synuclein immunoreactivity in retinas of transgenic mice. There was no pSer129 or total α-synuclein immunoreactivity detected in control retinas (Fig. 2A, B). In retinas of all 5-month-old transgenic mice, pSer129 immunoreactivity was evident only in the outer nuclear layer (Fig. 2C). Compared to total α-synuclein, pSer129 immunoreactivity was sparse, with two to three patches of labeling per retinal section of all mice (Fig. 2C, D). Retinas of inoculated 5-month-old transgenic mice demonstrated upregulated pSer129 immunoreactivity, compared to 5-month-old non-inoculated mice (Fig. 2C, E). In retinas of inoculated mice, pSer129 immunoreactivity was detected throughout the outer segments of photoreceptor cells, outer nuclear layer, outer plexiform layer, and inner nuclear layer, demonstrating accelerated accumulation of α-synuclein in the seeded model (Fig. 2C, E). Compared to control, retinas of 8-month-old and clinically ill transgenic mice had α-synuclein labeling similar to that of inoculated 5-month-old mice (Fig. 2G–L). In retinas of 8-month-old mice, pSer129 immunoreactivity was only evident in the outer nuclear layer, compared to total α-synuclein immunoreactivity that was also present in the inner retina (Fig. 2I, J). Retinas of clinically ill mice had similar distribution of pSer129 immunoreactivity throughout the outer and inner retina (Fig. 2K, L). In all micrographs, p129S and total α-synuclein immunoreactivity was more robust in the outer retina, compared to the inner retina. Western blot analysis of p129S and total α-synuclein protein levels produced similar results. Retinas of 8-month-old, clinically ill, and inoculated 5-month-old mice, had significantly more α-synuclein (~2 fold compared to control and 5-month-old transgenic mice; Fig. 2M, N). Our results indicated no significant difference in pSer129 accumulation among 8-month-old transgenic, clinically ill, or inoculated 5-month-old mice, suggesting that seeding of α-synuclein from the brain to the retina results in accelerated accumulation of the misfolded protein.

3.2. Activation of Müller glia in response to α-synuclein accumulation

To determine activation of Müller glia in response to misfolded protein accumulation, we assessed the distribution of GFAP immunoreactivity using immunohistochemistry. Müller glia are the principal glial component of the retina, responding to injury by increasing GFAP expression in processes radially through the thickness of the retina (Bringmann et al. 2006). GFAP immunoreactivity in retinas of control mice was localized to the Müller glia end feet and astrocytes in the optic fiber layer (Fig. 3A, D). Retinas of 5-month-old non-inoculated, and 5-month-old inoculated, and 8-month-old transgenic mice had comparable GFAP immunoreactive processes spanning the retina from the optic fiber layer to the outer plexiform layer (Fig. 3B, C, E). Retinas of clinically ill mice had robust Müller glial activation with hypertrophied Müller glia end feet, and GFAP immunoreactive processes detectable in the outer nuclear layer (Fig. 3F). When quantified, the area of GFAP immunoreactivity accounted for 13.99 ± 0.86% (TgM83 5 m), 13.32 ± 1.19% (inoculated TgM83 5 m), 10.40 ± 1.21% (TgM83 8 m), or 23.41 ± 2.17% (clinical TgM83 12-18 m) of total area (Fig. 3G). Activation of Müller glia was first detected in retinas of 5-month-old TgM83 mice and was significantly increased in retinas of 8-month-old and clinically ill mice. Compared to non-inoculated mice, retinas of 5-month-old inoculated mice did not have increased GFAP, suggesting that α-synuclein seeding did not have a detectable effect on activation of Müller glia.

3.3. TgM83 mice exhibit pTau^{Thr231} accumulation in retinal neurons and Müller glia

To determine whether the α-synuclein (A53T) gene mutation leads to accumulation of tau, an antibody against AT-180 (pThr231) was used for an immunohistochemical analysis. Tau protein plays a critical role in microtubule assembly, axonal transport, and neurite outgrowth, and is a major component of neurofibrillary tangles (NFTs) found in Alzheimer's disease (AD) and Parkinson's disease (PD) (Lei et al. 2010). Phosphorylated tau (pTau^{Thr231}) immunoreactivity was first appreciable in retinas of 5-month-old transgenic mice, with no pTau^{Thr231} immunoreactivity detected in retinas of corresponding control mice (Fig. 4A, B). Compared to non-inoculated mice, retinas of 5-month-old inoculated mice had greater pTau^{Thr231} immunoreactivity (~7-fold

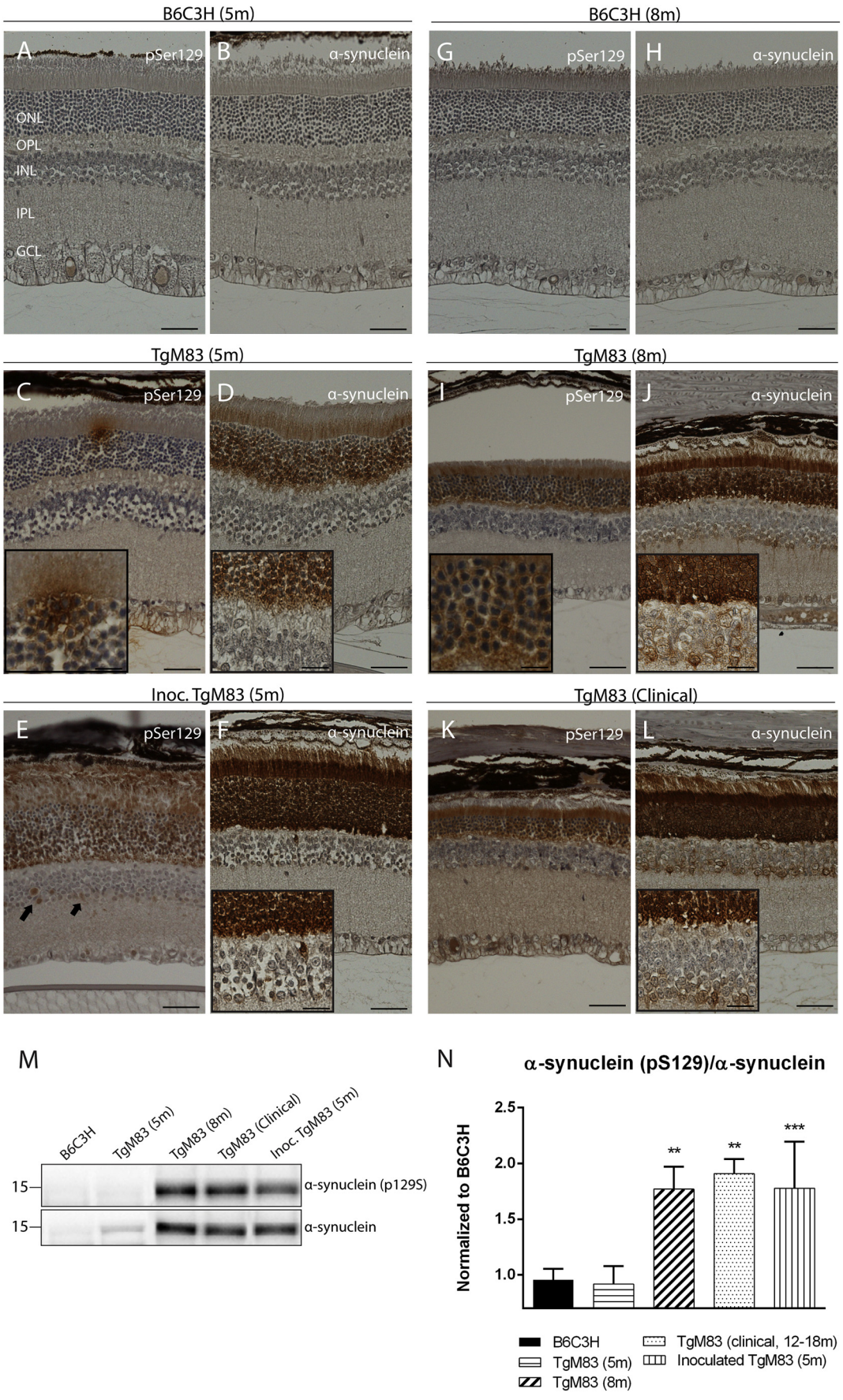

(caption on next page)

Fig. 2. Accumulation of α-synuclein. (A, B) Retinas of B6C3H mice had no phospho-α-synuclein (p129S) immunoreactivity. (C-F) Retinas of transgenic mice showed a similar trend, with sparse perinuclear and extracellular phospho α-synuclein (p129S) immunoreactivity at 5 months of age, evident in the inner retina at the stage of clinical disease. (E) Retinas of inoculated mice showed increased α-synuclein (p129S) immunoreactivity, localized to ONL as well as the inner retina. (G, H) Retinas of B6C3H mice had no α-synuclein immunoreactivity. (I) Perinuclear and extracellular α-synuclein accumulation first evident at 5 months of age, localized to ONL. (J-L) As disease progressed, α-synuclein accumulation increased in intensity, distributed throughout the inner retina. (K) Retinas of inoculated TgM83 mice are comparable to retinas of clinically ill TgM83 mice, with α-synuclein localized to ONL and inner retina. Abbreviations: GCL, ganglion cell layer; INL, inner nuclear layer; IPL, inner plexiform layer; OPL, outer plexiform layer; ONL, outer nuclear layer. Insets: High magnification images of α-synuclein immunoreactivity. Scale bars: 40 μm; insets 15 μm. (M) α-synuclein (pS129) (15 kDA), α-synuclein (15 kDA), immunoreactive bands. (N) Representative bar graph showing quantitative densitometric analysis of α-synuclein (pS129)/α-synuclein ± SD $^{**}P < 0.01$ vs. B6C3H and TgM83 (5 m); $^{***}P < 0.001$ vs. B6C3H and TgM83 (5 m).

higher), localized to the outer plexiform layer, ganglion cell layer, and optic fiber layer (Fig. 4C, E). Compared to retinas of age-matched control mice, those of 8-month-old transgenic mice had upregulated $pTau^{Thr231}$ immunoreactivity (Fig. 4D, E), although significantly less than retinas of inoculated, and clinically ill transgenic mice (Fig. 4C, F). When quantified, phosphorylated tau immunoreactivity comprised 1.11 ± 0.26% (TgM83 5 m), 8.02 ± 0.82% (inoculated TgM83 5 m), 2.63 ± 0.54% (TgM83 8 m), or 6.71 ± 1.53% (clinical TgM83 12-

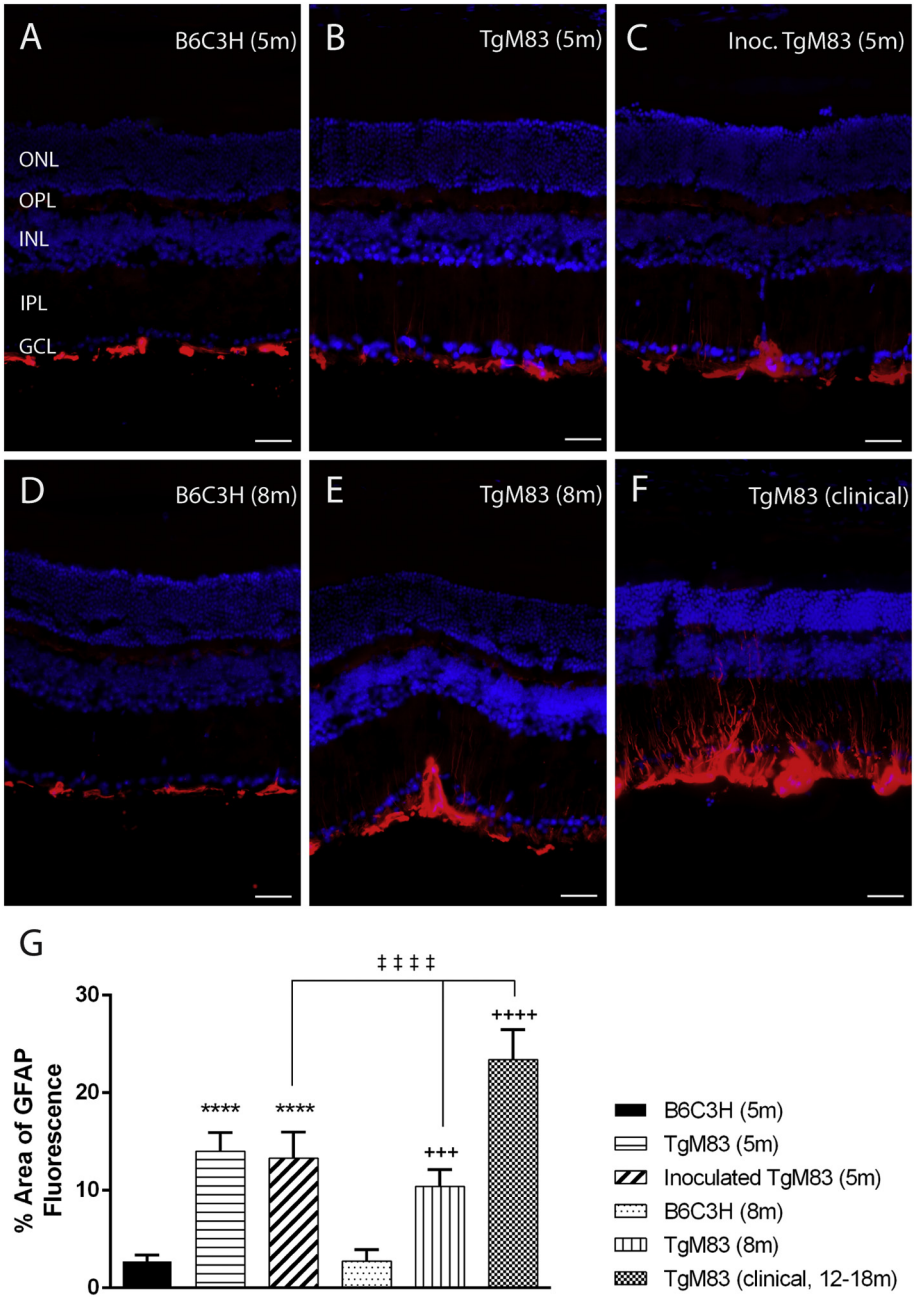

Fig. 3. Activation of Müller glia. (A, D) GFAP is localized to end feet of Müller glia in retinas of control mice. (B, C, E, F) Distribution of GFAP immunoreactivity is increased, spanning the entire thickness of the retina. (G) Bar graphs show significant increase in GFAP immunoreactivity in retinas of transgenic mice. Data are expressed as mean ± SD. Abbreviations: GCL, ganglion cell layer; INL, inner nuclear layer; IPL, inner plexiform layer; OPL, outer plexiform layer; ONL, outer nuclear layer. Scale bars: 20 μm. $^{****}P < 0.0001$ versus B6C3H (5 m); $^{+++}P < 0.001$ versus B6C3H (8 m); $^{++++}P < 0.0001$ versus B6C3H (8 m); $^{‡‡‡‡}P < 0.0001$.

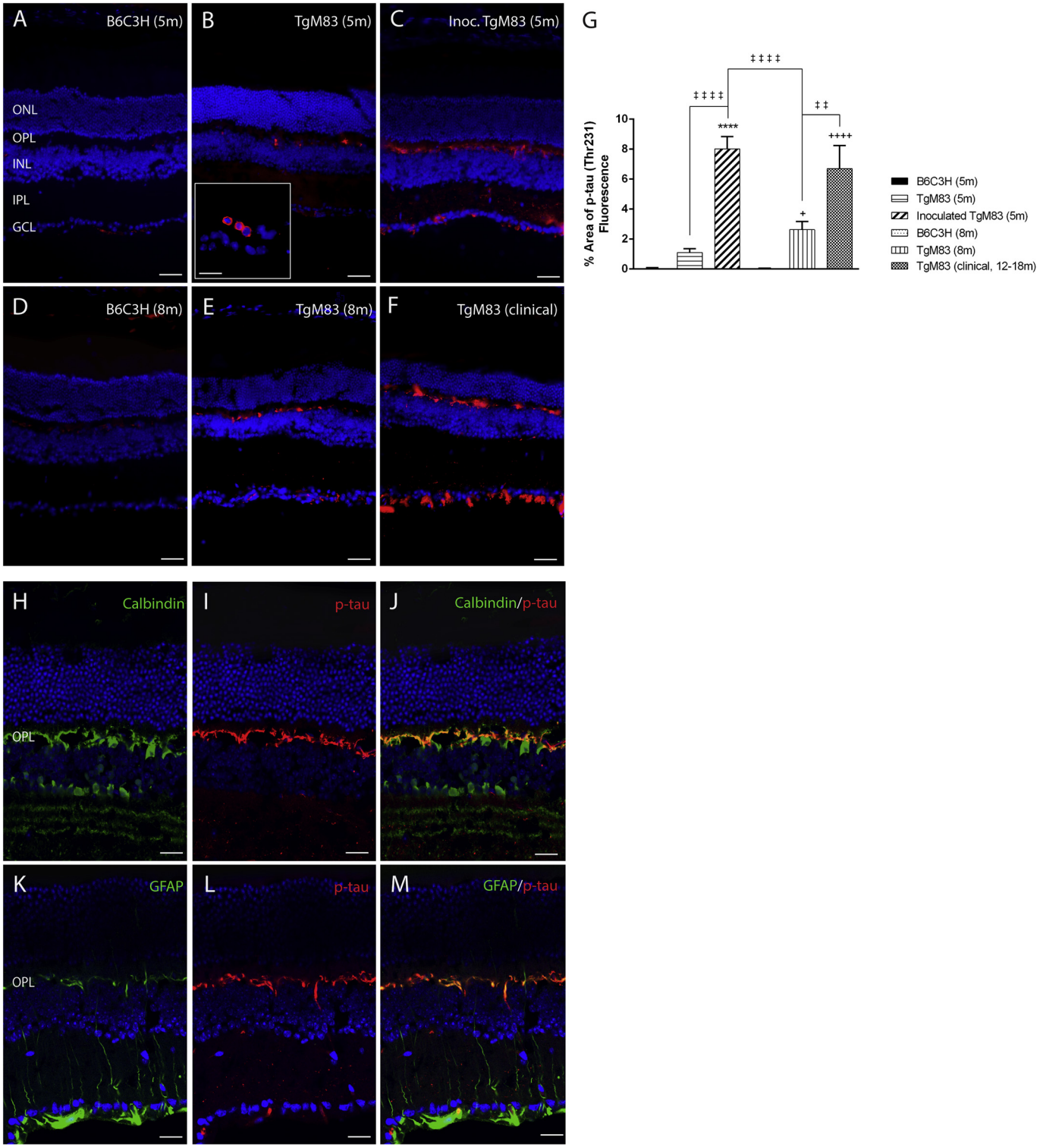

Fig. 4. Accumulation of phosphorylated tau. (A, D) No pTau^{Thr231} immunoreactivity was detectable in retinas of control mice. (B) pTau^{Thr231} immunoreactivity was first appreciable in retinas of transgenic mice at 5 months of age, localized to OPL and GCL. (C, E, F) Perinuclear pTau^{Thr231} accumulation is increased as disease progressed. (C) pTau^{Thr231} in retinas of inoculated TgM83 mice was comparable to retinas of TgM83 mice at clinical stage of disease. (G) Bar graphs show percent area of fluorescence for pTau^{Thr231}. Data are expressed as mean ± SD. (H-M) Confocal microscopy shows colocalization of GFAP and AT180 and of calbindin and AT180, suggesting that tau (pThr231) is present in Müller glial processes, and calbindin immunoreactive horizontal cells and photoreceptor cell terminals, respectively. Abbreviations: GCL, ganglion cell layer; INL, inner nuclear layer; IPL, inner plexiform layer; OPL, outer plexiform layer; ONL, outer nuclear layer. Inset: High magnification image of perinuclear pTau^{Thr231} localized in GCL. Scale bars: A-F 25 µm; H-M 15 µm; C inset 5 µm. ****P < 0.0001 versus B6C3H (5 m); $^{+}P < 0.05$ versus B6C3H (8 m); $^{++++}$P < 0.0001 versus B6C3H (8 m); ‡‡P < 0.01; ‡‡‡‡P < 0.0001.

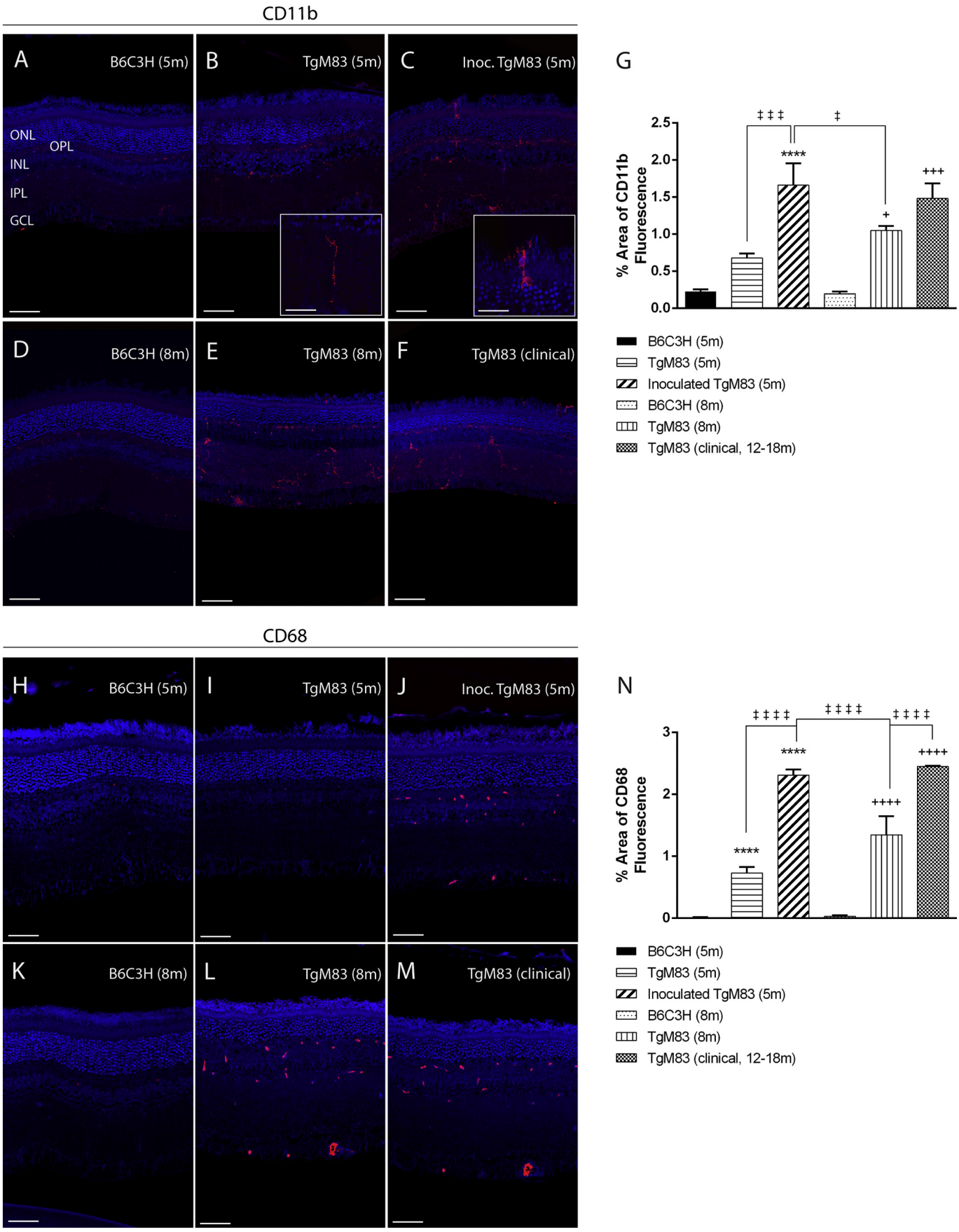

(caption on next page)

Fig. 5. Microglial activation. (A, B) Microglia of B6C3H and TgM83 (5 m) are quiescent, with long processes and small cell bodies, localized primarily to the plexiform layers. (C-F) Robust microglial activation is evident in retinas of TgM83 mice (8 m, inoculated, and clinical). Activated microglia have large cell bodies, thick or retracted processes, and appear to invade nuclear layers, and the outer segments of photoreceptor cells. (H-M) CD68 immunoreactivity shows activated and phagocytic microglia localized to the inner retina, compared to the lack of activated microglia in control retinas. (J, M). Microglial activation in inoculated TgM83 mice seems accelerated, as it is comparable to that of clinical disease. (G, N) Bar graphs show percent area of fluorescence for CD11b and CD68. Data are expressed as mean ± SD. Abbreviations: GCL, ganglion cell layer; INL, inner nuclear layer; IPL, inner plexiform layer; OPL, outer plexiform layer; ONL, outer nuclear layer. Insets: High magnification images of changes in microglial morphology due to activation. Scale bars: 20 μm; insets 5 μm. (G) ****P < 0.0001 versus B6C3H (5 m); $^{+}$P < 0.05 versus B6C3H (8 m); $^{+++}$P < 0.001 versus B6C3H (8 m); ‡P < 0.05; ‡‡‡P < 0.001. (N) ****P < 0.0001 versus B6C3H (5 m); $^{+++}$P < 0.001 versus B6C3H (8 m); ‡‡‡‡P < 0.0001.

18 m) of total area (Fig. 4G). The outer plexiform layer contains neuronal processes of horizontal cells that synapse with terminal regions of rods and cones (rod spherules and cone pedicles). Double immunofluorescence and confocal microscopy was used to confirm colocalization of pTau^{Thr231} with calbindin immunoreactive processes in the outer plexiform layer (Fig. 4H–J). Retinas of 5-month-old inoculated mice showed colocalization of immunofluorescence for calbindin and AT-180 (pThr231) in the outer plexiform layer. Since the pattern of AT-180 immunoreactivity in the outer plexiform layer was also similar to processes of activated Müller glia, double labeling with GFAP and AT-180 was used to confirm co-localization of GFAP and AT-180 in the outer plexiform layer. Retinas of 5-month-old inoculated mice had colocalization of immunofluorescence for GFAP and AT-180 (pThr231) in the outer plexiform layer. This data describes accumulation of phosphorylated tau in processes of neurons and retinal Müller glia, first detected at 5 months of age. This was coincident with the first detection of pSer129 in retinas of 5-month-old transgenic mice. Parallel to pSer129 immunoreactivity, pTau^{Thr231} was upregulated at 8 months and in clinically ill mice. Finally, we show significant upregulation of pTau^{Thr231} immunoreactivity in retinas of inoculated mice, compared to retinas of non-inoculated, suggesting accelerated tau phosphorylation in response to α-synuclein seeding.

3.4. Microglial activation parallels retinal degeneration due to accumulation of pSer129

To assess microglial activation, we performed immunohistochemistry using antibodies against CD11b and CD68. Upregulation of CD11b, the β-integrin marker of microglia, and macrophage antigen CD68 is associated with microglial activation in neuroinflammation (Crain et al. 2013; Roy et al. 2006; Walker and Lue 2015). In retinas of control mice, CD11b immunoreactive microglia had small somata with thin processes, sparsely dispersed through the outer and inner plexiform layers (Fig. 5A, D). CD11b immunoreactivity in retinas of 5- and 8-month-old control mice occupied 0.23 ± 0.03% and 0.20 ± 0.03% of total area, respectively (Fig. 5A, D, G). Compared to control retinas, CD11b immunoreactivity of transgenic mice at 5 months of age occupied 0.68 ± 0.06% of total area (Fig. 5A, B, G). Activated microglia were detected first in retinas of 8-month-old mice, shown by an increase in CD11b immunoreactivity and a change to an amoeboid like morphology (Fig. 5D, E). Retinas of inoculated 5-month-old mice, and clinically ill mice had significantly upregulated CD11b immunoreactivity, with large microglia often detected in the photoreceptor cell layer and outer segments (Fig. C, F). CD11b immunoreactivity occupied 1.05 ± 0.06%, and 1.48 ± 0.203%, and 1.67 ± 0.03% of total area, respectively (Figs. 5G). A similar trend was observed in CD68 immunoreactivity, with activated and phagocytic microglia localized to the inner retina of transgenic mice (Fig. 5H–N). Similar to CD11b, upregulated CD68 immunoreactivity was first evident in retinas of 8-month-old transgenic mice, occupying 1.35 ± 0.30% of total area (Fig. 5K, L). CD68 immunoreactivity was similar in retinas of clinically ill mice and those inoculated with brain homogenate, occupying 2.45 ± 0.01% and 2.31 ± 0.03% of total area, respectively (Fig. 5J, M, N). Results showed accelerated activation of CD11b^{+}/CD68^{+} microglia in retinas of 5-month-old inoculated mice, similar to microglial activation seen in retinas of clinically ill mice.

3.5. Dysregulation in retinal autophagy due to an increase in misfolded proteins

To assess the effect of accumulation of misfolded proteins on autophagy in the retina, we performed western blot and immunohistochemical analyses of proteins involved in initiation of autophagy and vesicle formation (Fig. 6A). In Parkinson's disease, an increase in autophagy is a proper response during clearing of bulk cytoplasmic contents, such as intracellular α-synuclein, however a decrease below basal levels indicates autophagic dysfunction (Klionsky et al. 2016; Lynch-Day et al. 2012). Conversely, a sustained increase of autophagosomes may also indicate an overload of a system that is incapable of clearing unwanted proteins (Klionsky et al. 2016; Lynch-Day et al. 2012). To determine changes in the initiation of autophagy, we examined the activation status of major autophagy-initiation proteins, pAMPK^{T172} and pULK1^{S757}, by western blot analysis. There was significant upregulation of pAMPK^{T172} protein levels in retinas of 5-month-old and 8-month-old transgenic mice, and a trending decrease in retinas of 5-month-old inoculated and clinically ill transgenic mice as compared to retinas of control B6C3H mice (Fig. 6B, C). Inversely, pULK1^{S757} protein levels were significantly lower in retinas of 5-month-old and 8-month-old transgenic mice, however they were upregulated in retinas of 5-month-old inoculated and clinically ill transgenic mice (Fig. 6B, D). To assess vesicle formation, we conducted western blot analysis and immunohistochemistry of autophagosome marker, LC3. Similar to pAMPK^{T172} protein levels, LC3 II protein levels were upregulated in retinas of 5-month-old and 8-month-old transgenic mice and downregulated in retinas of 5-month-old inoculated and clinically ill transgenic mice, compared to retinas of control mice (Fig. 6B, E). Immunohistochemistry results showed diffuse LC3 immunoreactivity in the outer and inner retina, suggesting an active basal level of autophagy ongoing under normal conditions (Fig. 6F). In retinas of 5-month-old transgenic mice, we saw significantly more LC3-immunoreactive autophagosomes, primarily localized to the outer nuclear layer and outer plexiform layer (Fig. 6G). In retinas of inoculated 5-month-old mice, we saw depletion of LC3 throughout the entire retina (Fig. 6H–J). This was similar to what was seen in retinas of 8-month-old and clinically ill mice (Fig. 6H, I). Taken together, these results show changes in macroautophagy associated with increased accumulation of pSer129 detected at clinical illness, or due to α-synuclein seeding. At earlier timepoints, there was an increase in autophagic activity, suggested by the increase in pAMPK^{T172} and LC3 II, and a decrease in pULK1^{S757}. However, in retinas of clinically ill mice and inoculated mice seeded with α-synuclein, we see autophagy similar to that of control mice, which suggests that an overloading of the autophagic system, by excessive α-synuclein accumulation, may lead to its ultimate dysfunction.

3.6. Photoreceptor cell death in α-synuclein associated retinopathy

To determine if there was photoreceptor cell loss, we assessed the thickness of the outer nuclear layer, as measured by number of photoreceptor cell nuclei. The mean thickness of the outer nuclear layer of

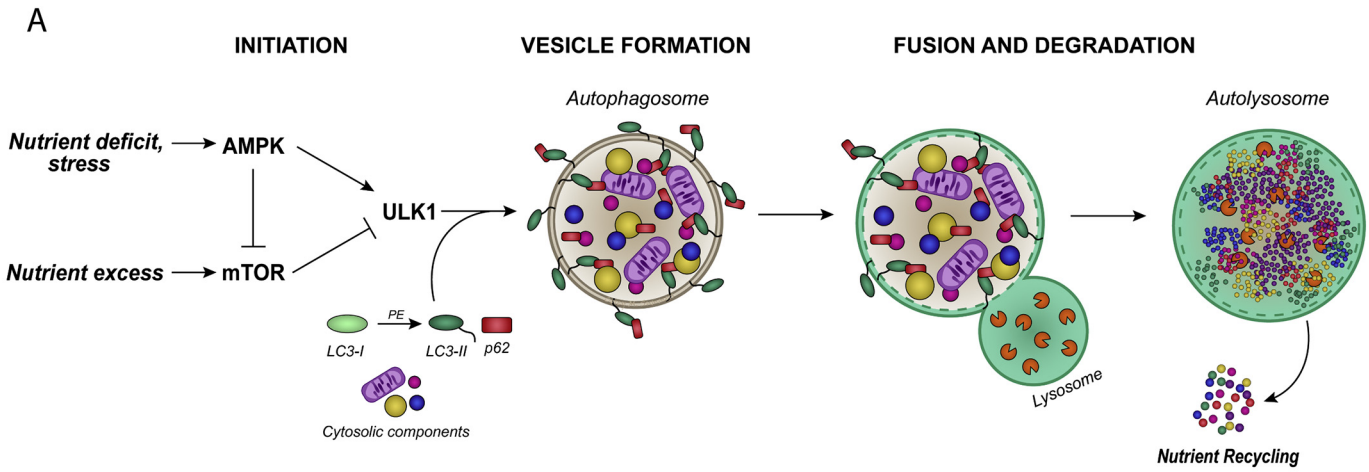

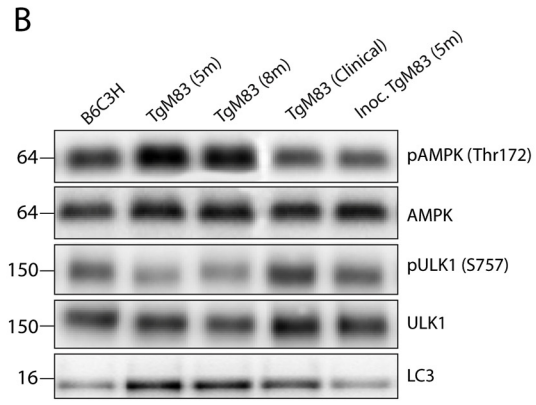

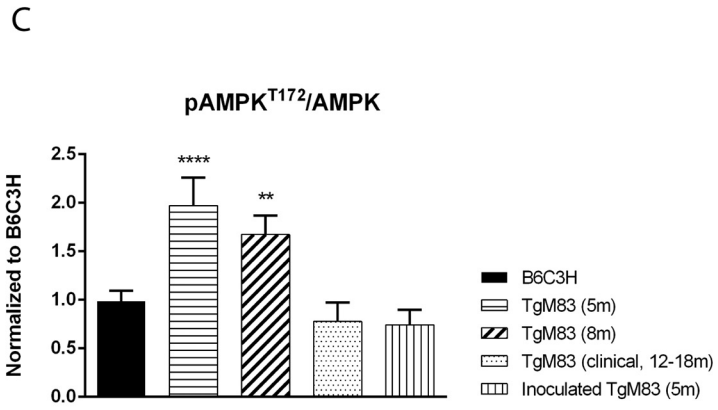

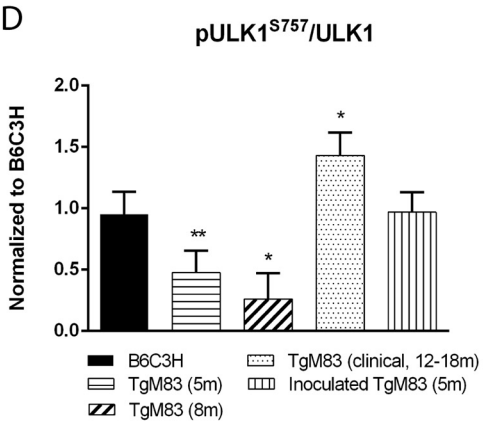

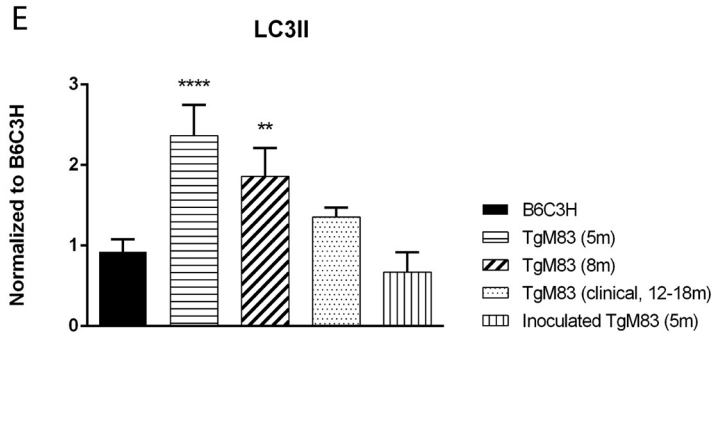

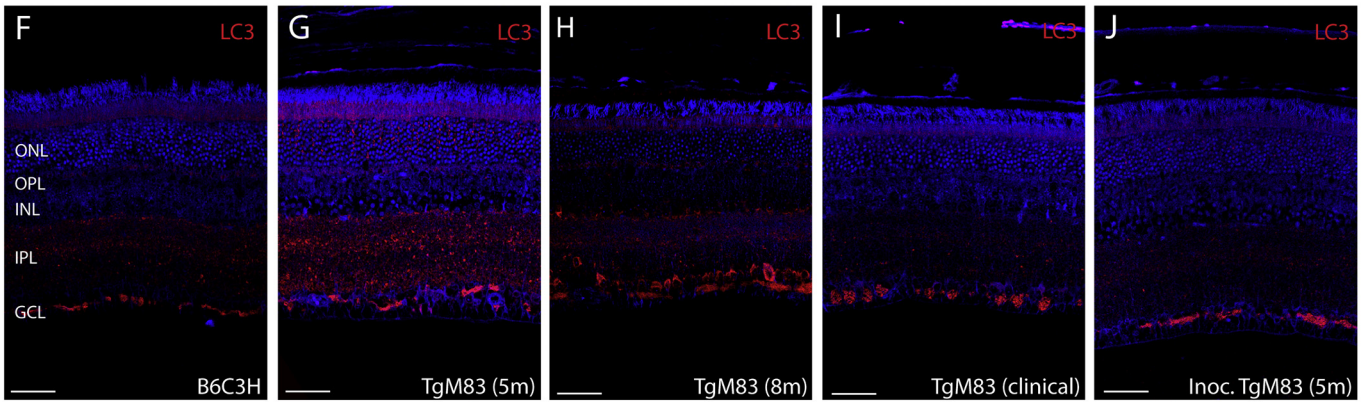

(caption on next page)

Fig. 6. Dysregulation of autophagy. (A) Schematic diagram of autophagic progression, broken down into the general stages, including induction, autophagosome formation, and degradation. (B) Western blot analysis of $pAMPK^{T172}$, $pULK1^{S757}$, and LC3 expression levels in the retina. $pAMPK^{T172}$ (64 kDA), AMPK (64 kDA), $pULK1^{S757}$ (150 kDA), ULK1 (150 kDA), and LC3 (14,16 kDA) immunoreactive bands. (C-E) Representative bar graphs showing quantitative densitometric analysis of $pAMPK^{T172}$/AMPK ± SD (I); $pULK1^{S757}$/ULK1 ± SD (J); LC3 II/total protein ± SD (K) in retinas of all mice. *P < 0.05; **P < 0.01; ****P < 0.0001. (F) Diffuse LC3 immunoreactivity in retinas of control mice is representative of basal autophagy (G) Increase in LC3-immunoreactive autophagosomes in ONL and OPL evident in retinas of TgM83 (5 m) mice is suggestive of normal autophagic response to disease. (H-J) Retinas of TgM83 (8 m), Inoculated TgM83 (5 m), and clinically ill mice show an appreciable decrease in LC3-immunoreactive puncta, similar to control retinas with basal autophagy. Abbreviations: GCL, ganglion cell layer; INL, inner nuclear layer; IPL, inner plexiform layer; OPL, outer plexiform layer; ONL, outer nuclear layer. Scale bars: 40 μm. Data are expressed as means ± SD. *P < .05 versus B6C3H (5 m); $^{++++}$P < .0001 versus B6C3H (8 m); ‡P < .05; ‡‡‡‡P < .0001.

age-matched control B6C3H mice were 14.50 ± 0.22 and 13.00 ± 0.36 cell nuclei, respectively (Fig. 7A). Outer nuclear layer thickness was comparable between 5-month-old non-inoculated and inoculated transgenic mice, with 13.40 ± 0.40 and 13.2 ± 0.37 cell nuclei, respectively (Fig. 7A). Photoreceptor cell loss was evident in retinas of 8-month-old and clinically ill transgenic mice (Fig. 7A). Mean outer nuclear layer thickness in retinas of 8-month-old transgenic mice was 8.50 ± 0.50 cell nuclei (35% decrease compared to age-matched control), while outer nuclear layer thickness in retinas of clinically ill mice was 5.50 ± 0.50 cell nuclei (70% decrease compared to retinas of control mice; Fig. 7A). Caspase-3 is an important mediator of neuronal apoptosis and plays a pivotal role in pathologic death in the CNS due to Parkinson's Disease. To determine if caspase-3 activation preceded photoreceptor cell degeneration due to the A53T mutation, we used cleaved anti-caspase-3 as an indicator of apoptosis. Retinas of B6C3H mice had no detectable caspase-3 labeling, while those of 8-month-old and clinically ill mice had caspase-3 immunoreactivity in both the outer nuclear layer and outer segments of photoreceptor cells (Fig. 7B–D). Detectable caspase-3 immunoreactivity coincided with retinal outer nuclear layer thinning, suggesting the potential role of caspase-3 in A53T mutation induced photoreceptor cell death.

3.7. A53T mouse model of synucleinopathy does not show changes in retinal tyrosine hydroxylase immunoreactivity

Tyrosine hydroxylase (TH) catalyzes the formation of L-DOPA in the biosynthesis of dopamine, therefore loss of TH activity followed by a loss of the protein is classically contributed to dopamine deficiency and phenotypic expression in PD (Joyce et al. 1997). To determine whether TH-expressing (dopaminergic) cells in the retina were affected due to the A53T mutation, immunohistochemistry was performed using anti-tyrosine hydroxylase. TH immunoreactivity was comparable in all retinas, with approximately one to four amacrine cell bodies in the inner nuclear layer of each retinal section and thick dendritic processes in the IPL (Fig. 7E–J). Results showed no changes in TH-immunoreactive amacrine cells.

3.8. Raman spectroscopic analysis can differentiate between spectral signatures of normal and diseased retinas

To detect biochemical differences in the retinal ganglion cell layers of healthy and diseased mice, we measured 20 spectra from 20 cells within the ganglion cell layer of 6 groups of mice, for a total of 400 spectra from each group. Ganglion cells were used for analysis because they are the innermost (closest to the lens) cellular layer of the retina. The Raman spectra reflects the molecular make up of a specific sample, with contributions from functional groups of major macromolecules that make up cells, i.e., proteins, RNAs, and DNAs. Fifteen of the 20 spectra were used to train a classifier, and 5 were used to test the classifier. The mean classification accuracy ± SD, was then calculated to determine how well the classifier could distinguish between two pairs of samples (Table 1). Our data demonstrates a high classification accuracy between retinal ganglion cells of control (B6C3H 5 months and 8 months) and transgenic mice (TgM83 5 months and 8 months), 89.33 ± 5.43% and 92.00 ± 4.73%, respectively. We also observed high classification accuracies between retinal ganglion cells of retinas that were histologically similar [i.e. retinal ganglion cells of inoculated 5-month-old mice (Inoc. TgM83 5 m) and clinically ill mice (TgM83 clinical) were accurately distinguishable 75.00 ± 3.23% of the time, and retinal ganglion cells of 8-month-old mice (TgM83 8 m) and clinically ill mice were accurately distinguishable 90.00 ± 6.0% of the time]. The lowest classification accuracy (75.00 ± 3.23%) was observed when comparing tissues that were the most histologically similar, specifically retinas of clinically ill and inoculated mice. These results suggest that Raman spectroscopy can effectively discriminate between retinal ganglion cells of healthy and diseased mice and is sensitive enough to differentiate between retinas that are otherwise histologically indistinguishable when analyzing α-synuclein immunoreactivity, $pTau^{Thr231}$ immunoreactivity, and microglial activation.

4. Discussion

4.1. Accumulation of pSer129 is accelerated in retinas of seeded mice

Our results demonstrate that pSer129, the principal protein modification in α-synuclein critical in the pathogenesis of Parkinson's disease, is expressed widely in retinas of transgenic mice (TgM83). In human patients, the earliest report of α-synuclein accumulation in the retina describes α-synuclein aggregates localized to the inner retina of postmortem PD patients (Bodis-Wollner et al. 2014). Additionally, a live imaging study revealed accumulation of α-synuclein deposits in retinal ganglion cells of α-synuclein::GFP mice in a model of Parkinson's disease (Price et al. 2016). A recent study described accumulation of phosphorylated α-synuclein deposits in the inner retina of human PD and Lewy body disease subjects, similar to Lewy bodies and Lewy neurites that occur in the brain (Ortuño-Lizarán et al. 2018). Our work describes outer and inner retinal accumulation of pSer129 due to the α-synuclein (A53T) gene mutation, which has not yet been reported in humans. We see detectable accumulation of pSer129 at 5 months of age, localized to the photoreceptor cell layer. Accumulation of pSer129 in the inner retina is detected in clinically ill mice and 5-month-old mice seeded with α-synuclein. Similar localization is observed with total α-synuclein, detected at 5 months of age in the photoreceptor cell layer, then in the inner retina at 8 months of age. Our results also show that seeding accelerates the disease process in the retina, as the pattern and magnitude of pSer129 protein accumulation was almost indistinguishable between inoculated 5-month-old mice and clinically ill mice. To gauge the effects of injection-related neuroinflammation, several studies report that inoculation of brain homogenate from healthy TgM83 mice fails to accelerate synucleinopathy (Luk et al. 2012b; Mougenot et al. 2012; Sargent et al. 2017).

We show, for the first time, that inoculation of brain homogenate of affected mice into young transgenic mice causes a prominent acceleration of retinal pSer129 accumulation, consistent with a “prion-like” propagation of α-synuclein highlighted in many works (Angot et al. 2010; Katorcha et al. 2017; Luk et al. 2012a; Masuda-Suzukake et al. 2013; Mougenot et al. 2012; Woerman et al. 2017). Mougenot et al. report accumulation of diffuse α-synuclein (pSer129) inclusions in brains of TgM83 mice inoculated with brain homogenates from

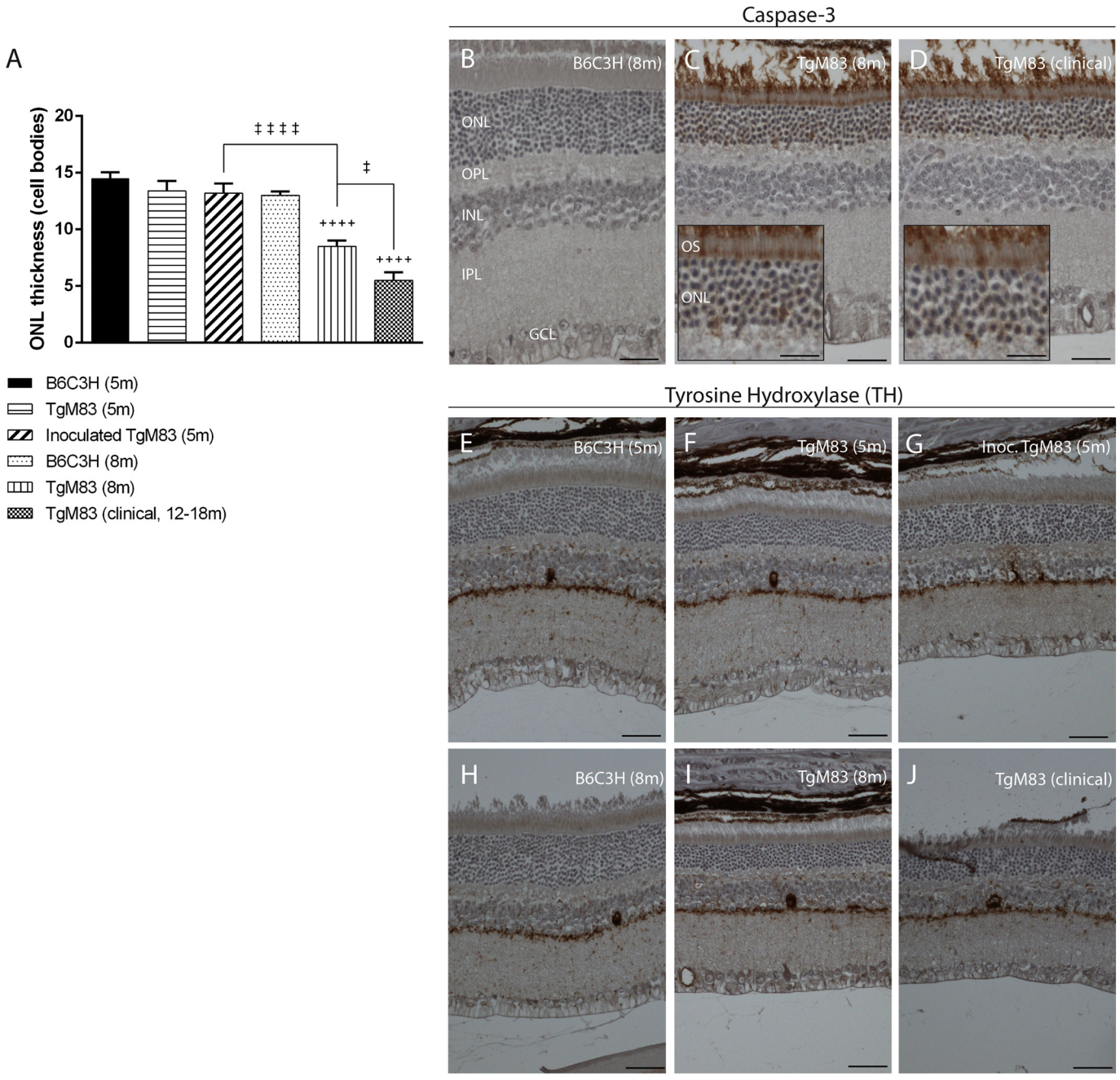

Fig. 7. Neuronal loss. (A) A53T mutation causes progressive photoreceptor cell death evident first at 8 months of age. Photoreceptor cell loss is also evident in retinas of inoculated TgM83 (5 m). (B-D) No caspase-3 labeling is seen in retinas of B6C3H mice, while caspase-3 immunoreactive photoreceptor cells are evident in retinas of 8-month-old and clinically ill mice, indicating apoptotic cell death. (*E-J*) Tyrosine hydroxylase immunoreactivity was comparable among all mouse groups. Abbreviations: GCL, ganglion cell layer; INL, inner nuclear layer; IPL, inner plexiform layer; OPL, outer plexiform layer; ONL, outer nuclear layer. Scale bars: 40 µm. Data are expressed as means ± SD. *P < .05 versus B6C3H (5 m); $^{++++}$P < .0001 versus B6C3H (8 m); ‡P < .05; ‡‡‡‡P < .0001.

Table 1
Mean classification accuracies ± SD for retinal ganglion cells between a paired set of samples.

	TgM83 5 m	TgM83 8 m	Inoc. TgM83 5 m	B6C3H 5 m	B6C3H 8 m
TgM83 8 m	88.00 ± 3.50%				
Inoc. TgM83 5 m	89.56 ± 2.64%	89.71 ± 2.91%			
B6C3H 5 m	89.33 ± 5.43%	88.86 ± 6.32%	90.00 ± 4.22%		
B6C3H 8 m	91.71 ± 3.49%	92.00 ± 4.73%	93.67 ± 2.77%	83.50 ± 5.02%	
TgM83 clinical	94.57 ± 4.86%	90.00 ± 6.00%	75.00 ± 3.23%	90.33 ± 3.48%	89.00 ± 3.00%

clinically ill TgM83 mice, as well as early occurrence of clinical signs and smaller survival times (Mougenot et al. 2012). An increasing amount of in vitro and in vivo evidence argues that neurodegenerative diseases, including Parkinson's disease, Alzheimer's disease, multiple system atrophy (MSA), and progressive supranuclear palsy (PSP), are in fact prion-like diseases, in which misfolded proteins (e.g. α-synuclein and tau) undergo self-propagation. Although, it is important to note that for example, α-synuclein prions in PD are distinct from prions in other synucleinopathies (Luk et al. 2012a; Prusiner et al. 2015; Woerman et al. 2016; Woerman et al. 2015; Woerman et al. 2017), therefore may behave differently depending on disease.

4.2. Microglial and Müller glial activation differs in response to α-synuclein seeding

The first detection of pSer129 in the retina was accompanied by up-regulation of GFAP in Müller glia, perhaps an early indicator of retinal stress in response to the presence of α-synuclein. GFAP immunoreactivity was significantly higher in retinas of 8-month-old and clinically ill mice, and parallel to increased pSer129 accumulation at those time points. Activation of Müller glia is a ubiquitous response observed in many retinal diseases (Bringmann and Reichenbach 2001), however this observation has not been previously reported in α-synuclein related retinopathy. Consistent with these results, we have previously described activation of Müller glia that was coincident with the earliest detection of retinal misfolded prion protein in a mouse model of misfolded protein transport and accumulation (Greenlee et al. 2016). Interestingly, GFAP immunoreactivity in retinas of 5-month-old inoculated mice and age-matched non-inoculated mice were comparable, suggesting that α-synuclein "seeding" did not have a detectable effect on activation of Müller glia. However, altered microglial morphology and retinal neuroinflammation demonstrated by the microglia specific markers, CD11b and CD68, were better indicators of disease acceleration. A significant increase in CD11b immunoreactivity was first detected in retinas of 8-month-old transgenic mice, concurrent with robust CD68 immunoreactivity localized to the outer and inner retina. Both CD11b and CD68 immunoreactivity was higher in retinas of clinically ill mice and retinas of 5-month-old inoculated mice, suggesting acceleration of retinal neuroinflammation in response to α-synuclein accumulation. These results were also supported by changes in microglial morphology. We observed reactive microglia with large cell bodies and retracted processes with an amoeboid like appearance in retinas of clinically-ill and 5-month-old inoculated mice, while retinas of non-inoculated 5-month-old mice had microglia with small cell bodies and long bipolar processes indicative of a ramified, non-activated state. The contribution of microglia-mediated neuroinflammation to retinal degenerative diseases is widely known (Madeira et al. 2015), however our work describes dynamic changes in cell surface markers and morphology of microglia in response to α-synuclein accumulation that has not been previously reported in the retina. Numerous studies using transgenic α-synuclein animal models link α-synuclein exposure to MHCII-dependent microglia-mediated neuroinflammation, including inflammatory cytokine release, increased oxidative and nitrosative stress, and subsequent dopaminergic cell death (Schapansky et al. 2015; Sekiyama et al. 2012). Although chronic microglial activation is a detrimental contributor to neurodegenerative diseases, such as Parkinson's disease and Alzheimer's disease (reviewed in (Polazzi and Monti 2010)), clearance and degradation of α-synuclein is a pivotal measure taken by microglia to not only prevent the spread of α-synuclein, but perhaps actively avert α-synuclein internalization and deposition into neurons (Lee et al. 2008; Rey et al. 2013). Acceleration of microglial activation in seeded mice may correspond to the phagocytic nature and superior scavenging capabilities of microglia that are absent in Möller glia, suggesting that microglial activation may be a more sensitive indicator of retinal disease progression.

4.3. Increased accumulation of $pTau^{Thr231}$ in the retina coincides with accumulation of pSer129

A hallmark feature of neurodegenerative diseases, including Parkinson's disease (PD) and Alzheimer's disease (AD), is the accumulation of hyper-phosphorylated tau in the form of neurofibrillary tangles in both neurons and glial cells (Lee et al. 2001). One study described $pTau^{Thr231}$ accumulation in retinal ganglion cells in a mouse model of Alzheimer's disease (AD), suggesting a prominent role for aberrant tau in retinal neuron dysfunction and visual defects experienced by patients (Chiasseu et al. 2017). We have previously reported the accumulation of $pTau^{Thr231}$ in retinal neurons and glia in a mouse model of traumatic brain injury (Mammadova et al. 2017). Elevated levels of hyperphosphorylated tau have been previously reported in the striata of adult A53T mutant mice (Oaks et al. 2013; Wills et al. 2011). Another study described the colocalization of tau oligomers with astrocytes and microglia in retinas of Alzheimer's disease (AD) and frontotemporal lobar dementia (FTLD) patients, suggesting a detrimental relationship between the spread of tau oligomers and neuroinflammation (Nilson et al. 2017). Thus far, the accumulation of tau in the retina has not been described in a model of Parkinson's disease.

Our work demonstrates p-tau^{Thr231} accumulation in processes of retinal neurons and Möller glia, appreciable at 5 months of age. Phosphorylation of tau on Thr231, described as "pre-tangle" tau, has been shown to inhibit tau's ability to bind and stabilize microtubules (Cho and Johnson 2004). Interestingly, the first detection of phosphorylated tau coincides with the first detection of α-synuclein (pSer129). Just as with pSer129, we see significantly higher $pTau^{Thr231}$ immunoreactivity in retinas of inoculated mice, suggesting accelerated accumulation of phosphorylated tau in response to α-synuclein seeding. The role of tau in the pathogenesis of PD is presently unknown, however evidence suggests a stimulatory effect of α-synuclein on tau phosphorylation (Kawakami et al. 2011). Due to the co-occurrence of tau and α-synuclein filamentous amyloid inclusions in human neurodegenerative diseases, *in-vivo* studies suggest that the interaction between α-synuclein and tau is synergistic and can promote hyper-phosphorylation and fibrillization in the TgM83 mouse model (Giasson et al. 2003). Studies propose that the interaction between α-synuclein and tau leads to specific and sequential phosphorylation events of the tau protein resulting in loss of function (decreased microtubule binding), as well as gain of function (abnormal tau-tau interactions), leading to tau dysfunction and accumulation into neurofibrillary tangles (Binder et al. 1985; de Calignon et al. 2012; Johnson and Stoothoff 2004; Lei et al. 2010). Moreover, an in vitro study demonstrates that misfolded α-synuclein displays a self-replicating, as well as a cross-seeding ability (i.e. aggregated α-synuclein can trigger misfolding of cellular prion protein) (Katorcha et al. 2017). Another *in-vitro* study reports that tau fibrils can induce intracellular tangle-like aggregates, suggesting seeding activity of misfolded tau as a potential mechanism of tau propagation *in vivo* (Guo and Lee 2011).

Our work is the first to describe accumulation of "pre-tangle" tau in retinal neurons and glia, due to the A53T α-synuclein gene mutation. Also, this work provides evidence that α-synuclein seeding may contribute to, and possibly accelerate the accumulation of $pTau^{Thr231}$ proteins in the retina. Although compelling, the mechanisms underlying the interaction of α-synuclein (pSer129) and tau require further investigation.

4.4. A decrease in autophagy is coincident with increased accumulation of α-synuclein, and $pTau^{Thr231}$

This work describes changes in retinal macroautophagy associated with the pathogenic A53T mutant α-synuclein, that have not been previously reported. Macroautophagy is the only known intracellular mechanism potentially capable of degrading bulk protein aggregates, although in mammals, all of the proteins involved and the precise

sequence of events are still not completely established (reviewed in (Jaeger and Wyss-Coray 2009)). Briefly illustrated in Fig. 6, the initiation stage involves activation of ULK1 (a serine-threonine kinase), regulated by both mTOR and AMPK. Activation of mTOR leads to the enzymatic inactivation of ULK1, by downstream phosphorylation at serine 757. Conversely, when AMPK is activated by phosphorylation at Threonine 172 and mTOR is inhibited, due to nutrient deficit or stress, ULK1 is dephosphorylated at Serine 757 and thereby activated allowing for autophagy to progress. Subsequently, lipidation of LC3 I to form LC3 II, and binding of specific adaptor proteins such as p62, contributes to autophagosome formation. Finally, fully formed autophagosomes fuse with lysosomes for degradation and recycling of cellular contents including organelles and proteins. Our results demonstrate two opposing events in the autophagic pathway: upregulation of the initiation of autophagy, suggested by the increase in $pAMPK^{T172}$ and LC3 II, along with the decrease in $pULK1^{S757}$ at "early" timepoints (retinas of 5-month-old and 8 months old mice); downregulation of autophagy at the "later" timepoint (retinas of clinically ill mice). Retinas of inoculated or "seeded" mice were almost indistinguishable from those of clinically ill mice, perhaps suggesting impaired autophagy due to an overload of the system by misfolded α-synuclein accumulation. Here, the upregulation event first detected in retinas of 5-month-old transgenic mice, coincides with the first detection of pSer129 and $pTau^{Thr231}$ accumulation, a proper response during clearing of cytoplasmic contents. Later, downregulation of autophagy seen in retinas of clinically ill and seeded mice, could suggest impaired autophagy due to an overload of misfolded proteins, α-synuclein and $pTau^{Thr231}$. In neurodegenerative diseases such as PD, AD, and Huntington's disease, autophagy is impaired (reviewed in (Jaeger and Wyss-Coray 2009)). Consistent with our results, the general hallmark effect of CNS disease on autophagy is the accumulation of autophagosome-like structures. However, whether autophagosome accumulation occurs due to an impairment in the degradation of autophagosomes, or due to an increased need for the clearance of unwanted intracellular contents, is not yet known. Specifically, in PD associated mutations A53T and A30P, a study demonstrated that α-synuclein inhibits chaperone-mediated autophagy (CMA) by binding to its receptor and preventing not only degradation of itself, but that of other autophagy substrates (Cuervo et al. 2004). It is also unknown whether abnormalities in the autophagy pathway are caused by mutant or misfolded proteins, or whether deficits in the degradation of misfolded proteins are yet another factor that leads to protein aggregation. The complex intricacies of the autophagic pathway in neurodegenerative diseases are far from being understood, however data presented in this study suggests it may play a role in the cellular response to misfolded proteins including α-synuclein (pSer129) and $pTau^{Thr231}$.

4.5. Loss of retinal neurons in α-synuclein associated disease

This study reports loss of photoreceptors first detected in retinas of 8-month-old transgenic mice, corresponding to widespread distribution of pSer129 in the outer nuclear layer. The first detection of pSer129 immunoreactivity in retinas of 5-month-old mice precedes retinal thinning detected in retinas of 8-month-old mice. This observation is supported by studies that demonstrate an increase in misfolded proteins before onset of pathological changes (Sandberg et al. 2014). Loss of photoreceptors also coincided with cleaved caspase-3 immunoreactivity, detectable in the outer nuclear layer and the outer segments of photoreceptor cells, which may suggest photoreceptor apoptosis. Photoreceptor cell loss in response to the accumulation of misfolded proteins has been previously reported in a seeded rodent model of scrapie, and similar to our observation, loss of retinal neurons did not occur until late in the disease long after the first detection of misfolded prion protein (Greenlee et al. 2016). Besides scrapie, the vulnerability of photoreceptor cells to the accumulation of misfolded proteins has also been shown in other models of transmissible spongiform encephalopathies (TSEs), including Creutzfeldt-Jacob disease (Hogan et al. 1983) and transmissible mink encephalopathy (Hogan et al. 1986), however photoreceptor cell death in response to α-synuclein accumulation has not been previously reported. Visual deficits in PD are often attributed to dopaminergic deficiency (Archibald et al. 2009), however our results demonstrate no detectable changes in tyrosine hydroxylase immunoreactivity in dopaminergic amacrine cells. While there is evidence of reduced tyrosine hydroxylase immunoreactivity in retinas of PD patients, this observation was made in five patients and has not been since examined (Nguyen-Legros 1988). Retinal dopamine deficiency in PD has not been since explored. Further studies are necessary to delineate the effect of α-synuclein on retinal dopamine, and whether this contributes to visual dysfunction in PD.

4.6. Raman spectroscopy can detect molecular changes in Parkinson's disease related retinopathy

In this study, we explored the potential of using Raman spectroscopy for differentiating retinal tissues of transgenic mice from those of healthy controls. Since our histological data demonstrated pathologic changes in retinas of transgenic mice, it was reasonable to hypothesize a difference in the molecular makeup of affected ganglion cells. For the first time in this study, spectroscopic markers associated with changes in α-synuclein related intracellular protein compositions in retinal ganglion cells were identified with high accuracy. Raman spectroscopy has been an invaluable tool facilitating several biomedical applications, including diagnostics and therapeutic development. For example, Raman spectroscopy is slowly making its way into clinics as a non-invasive way to characterize different cancers, by collecting biochemical information from in situ samples of tumors (Huang et al. 2005; Taleb et al. 2006). Raman spectroscopy has also been successfully used for the evaluation of glaucomatous retinal changes in canine tissues (Wang et al. 2011). Taken together with our results, Raman spectroscopic screening could potentially be used for early characterization of pathologic retinal changes due to a variety of neurodegenerative disorders. If further optimized and refined, and in combination with in vivo imaging techniques, Raman spectroscopy may be implemented to develop effective and safe early-diagnostic modalities for PD patients with deficits in vision.

5. Conclusions

In this study, we report retinal changes associated with the α-synuclein A53T mutation, as well as describe the effect of α-synuclein "seeding" on the development of retinal pathology. We demonstrate that pSer129 is first detected in retinas of transgenic mice at 5 months of age, then widely expressed in the outer and inner retina. This finding is consistent with the first detection of $pTau^{Thr231}$, and activation of retinal Müller glia and microglia. We report that microglial activation seems to be a more sensitive indicator of retinal stress, as we see a robust increase in microglial activation, but not activation of Müller glia, due to seeding. We show, for the first time, that seeding with brain homogenate from clinically ill mice, causes a prominent acceleration of retinal pSer129 and $pTau^{Thr231}$ accumulation. This finding is consistent with other works describing the self-propagating ability of misfolded proteins. Our work also suggests that seeding with brain homogenate from clinically ill mice leads to the dysfunction of protein degradation, and collapse of protein quality control systems leading to neuroinflammation and further accumulation of misfolded proteins. An increase in pSer129 and $pTau^{Thr231}$ accumulation may lead to dysregulation in retinal autophagy and cell death, however mechanistic studies are necessary to delineate direct effect of prion-like α-synuclein propagation from the detrimental effects of general cellular dysfunction specific to protein degradation. Finally, we provide evidence that Raman spectroscopy can be used to differentiate between retinal tissues from control, healthy, and diseased mice with high accuracy, even among retinas that appear histologically similar. If further refined,

successful implementation of this non-invasive and rapid technique can potentially replace histology as the current gold standard of synucleinopathy diagnosis, perhaps earlier in the disease process than is currently possible. Taken together, our work sheds light on the pathological events of Parkinson's disease in the retina that have not been previously reported.

Declaration of interest

None.

Animal rights

The animals were housed per group in enriched cages in a temperature-controlled room on a 12 h light/dark cycle, and received water and food ad libitum, in our approved facilities (No. C69 387 0801) for breeding and experimental studies, in accordance with EEC Directive 86/609/EEC and French decree No. 2013–118. The experimental studies described in this article were performed in containment level 3 facilities. Monitoring of the M83 mice in the experimental protocols is followed up by the Comite d'ethique CE2A – 16, ComEth ANSES/ENVA/UPEC.

Data statement

The datasets during and/or analyzed during the current study available from the corresponding author on reasonable request.

Funding

This work was supported by the Stem Cell Research Fund, Department of Genetics, Development, and Cell Biology, Department of Biomedical Sciences, and the National Animal Disease Center, USDA, Agricultural Research Service in Ames, Iowa.

Acknowledgements

The authors wish to thank Adrienne Shircliff, Judith Stasko, Virginia Montgomery, and Samantha Swift for technical assistance and Ekundayo Platt for early observations that lead to this work.

References

Angot, E., et al., 2010. Are synucleinopathies prion-like disorders? Lancet Neurol. 9, 1128–1138.
Archibald, N.K., et al., 2009. The retina in Parkinson's disease. Brain 132, 1128–1145.
Armstrong, R.A., 2011. Visual symptoms in Parkinson's disease. Parkinson's Dis. 2011.
Binder, L.I., et al., 1985. The distribution of tau in the mammalian central nervous system. J. Cell Biol. 101, 1371–1378.
Bodis-Wollner, I., 2013. Foveal vision is impaired in Parkinson's disease. Parkinsonism Relat. Disord. 19, 1–14.
Bodis-Wollner, I., et al., 2014. α-Synuclein in the inner retina in parkinson disease. Ann. Neurol. 75, 964–966.
Braak, H., et al., 2003. Staging of brain pathology related to sporadic Parkinson's disease. Neurobiol. Aging 24, 197–211.
Bringmann, A., Reichenbach, A., 2001. Role of Muller cells in retinal degenerations. Front. Biosci. 6, E72–E92.
Bringmann, A., et al., 2006. Müller cells in the healthy and diseased retina. Prog. Retin. Eye Res. 25, 397–424.
de Calignon, A., et al., 2012. Propagation of tau pathology in a model of early Alzheimer's disease. Neuron 73, 685–697.
Chen, L., et al., 2009. Tyrosine and serine phosphorylation of α-synuclein have opposing effects on neurotoxicity and soluble oligomer formation. J. Clin. Invest. 119, 3257.
Chiasseu, M., et al., 2017. Tau accumulation in the retina promotes early neuronal dysfunction and precedes brain pathology in a mouse model of Alzheimer's disease. Mol. Neurodegener. 12, 58.
Cho, J.H., Johnson, G.V., 2004. Primed phosphorylation of tau at Thr231 by glycogen synthase kinase 3β (GSK3β) plays a critical role in regulating tau's ability to bind and stabilize microtubules. J. Neurochem. 88, 349–358.
Crain, J.M., et al., 2013. Microglia express distinct M1 and M2 phenotypic markers in the postnatal and adult central nervous system in male and female mice. J. Neurosci. Res. 91, 1143–1151.
Cuervo, A.M., et al., 2004. Impaired degradation of mutant α-synuclein by chaperone-mediated autophagy. Science 305, 1292–1295.
Fujiwara, H., et al., 2002. α-Synuclein is phosphorylated in synucleinopathy lesions. Nat. Cell Biol. 4, 160–164.
Giasson, B.I., et al., 2003. Initiation and synergistic fibrillization of tau and alpha-synuclein. Science 300, 636–640.
Greenlee, M.H.W., et al., 2016. Temporal Resolution of Misfolded Prion Protein Transport, Accumulation, Glial Activation, and Neuronal Death in the Retinas of mice Inoculated with Scrapie. Am. J. Pathol. 186, 2302–2309.
Gunn, S.R., 1998. Support vector machines for classification and regression. ISIS technical report. 14, 5–16.
Guo, J.L., Lee, V.M.-Y., 2011. Seeding of normal Tau by pathological Tau conformers drives pathogenesis of Alzheimer-like tangles. J. Biol. Chem. 286, 15317–15331.
Hogan, R., et al., 1983. Retinal degeneration in experimental Creutzfeldt-Jakob disease. Lab. Investig. 49, 708–715.
Hogan, N., et al., 1986. Replication of scrapie prions in hamster eyes precedes retinal degeneration. Ophthalmic Res. 18, 230–235.
Huang, Z., et al., 2005. Raman spectroscopy in combination with background near-infrared autofluorescence enhances the in vivo assessment of malignant tissues. Photochem. Photobiol. 81, 1219–1226.
Jaeger, P.A., Wyss-Coray, T., 2009. All-you-can-eat: autophagy in neurodegeneration and neuroprotection. Mol. Neurodegener. 4, 16.
Johnson, G.V., Stoothoff, W.H., 2004. Tau phosphorylation in neuronal cell function and dysfunction. J. Cell Sci. 117, 5721–5729.
Joyce, J.N., et al., 1997. Differential modification of dopamine transporter and tyrosine hydroxylase mRNAs in midbrain of subjects with Parkinson's, Alzheimer's with parkinsonism, and Alzheimer's disease. Mov. Disord. 12, 885–897.
Katorcha, E., et al., 2017. Cross-seeding of prions by aggregated α-synuclein leads to transmissible spongiform encephalopathy. PLoS Pathog. 13, e1006563.
Kawakami, F., et al., 2011. Stimulatory effect of α-synuclein on the tau-phosphorylation by GSK-3β. FEBS J. 278, 4895–4904.
Klionsky, D.J., et al., 2016. Guidelines for the use and interpretation of assays for monitoring autophagy. Autophagy 12, 1–222.
Lee, V.M., et al., 2001. Neurodegenerative Tauopathies. Annual Review of Neuroscience. Vol. 24. pp. 1121–1159.
Lee, H.-J., et al., 2008. Assembly-dependent endocytosis and clearance of extracellular a-synuclein. Int. J. Biochem. Cell Biol. 40, 1835–1849.
Lei, P., et al., 2010. Tau protein: relevance to Parkinson's disease. Int. J. Biochem. Cell Biol. Vol. 42, 1775–1778.
Luk, K.C., et al., 2012a. Pathological α-synuclein transmission initiates Parkinson-like neurodegeneration in nontransgenic mice. Science 338, 949–953.
Luk, K.C., et al., 2012b. Intracerebral inoculation of pathological α-synuclein initiates a rapidly progressive neurodegenerative α-synucleinopathy in mice. J. Exp. Med. Jem. 209 (5), 975–986 (20112457).
Lynch-Day, M.A., et al., 2012. The role of autophagy in Parkinson's disease. Cold Spring Harbor Perspectives in Med. 2 (a009357).
Madeira, M.H., et al., 2015. Contribution of microglia-mediated neuroinflammation to retinal degenerative diseases. Mediat. Inflamm. 2015.
Mammadova, N., et al., 2017. Lasting Retinal Injury in a Mouse Model of Blast-Induced Trauma. Am. J. Pathol. 187, 1459–1472.
Masuda-Suzukake, M., et al., 2013. Prion-like spreading of pathological α-synuclein in brain. Brain 136, 1128–1138.
Mougenot, A.-L., et al., 2012. Prion-like acceleration of a synucleinopathy in a transgenic mouse model. Neurobiol. Aging 33, 2225–2228.
Nguyen-Legros, J., 1988. Functional neuroarchitecture of the retina: hypothesis on the dysfunction of retinal dopaminergic circuitry in Parkinson's disease. Surg. Radiol. Anat. 10, 137–144.
Nilson, A.N., et al., 2017. Tau oligomers associate with inflammation in the brain and retina of tauopathy mice and in neurodegenerative diseases. J. Alzheimers Dis. 55, 1083–1099.
Oaks, A.W., et al., 2013. Age-dependent effects of A53T alpha-synuclein on behavior and dopaminergic function. PLoS One 8, e60378.
Ortuño-Lizarán, I., et al., 2018. Phosphorylated α-synuclein in the retina is a biomarker of Parkinson's disease pathology severity. Mov. Disord. 1–10.
Polazzi, E., Monti, B., 2010. Microglia and neuroprotection: from in vitro studies to therapeutic applications. Prog. Neurobiol. 92, 293–315.
Price, D.L., et al., 2016. Longitudinal live imaging of retinal α-synuclein:: GFP deposits in a transgenic mouse model of Parkinson's Disease/Dementia with Lewy Bodies. Sci. Rep. 6, 29523.
Prusiner, S.B., et al., 2015. Evidence for α-synuclein prions causing multiple system atrophy in humans with parkinsonism. Proc. Natl. Acad. Sci. 112, E5308–E5317.
Recasens, A., Dehay, B., 2014. Alpha-synuclein spreading in Parkinson's disease. Front. Neuroanat. 8.
Rey, N.L., et al., 2013. Transfer of human α-synuclein from the olfactory bulb to interconnected brain regions in mice. Acta Neuropathol. 126, 555–573.
Ridder, A., et al., 2017. Impaired contrast sensitivity is associated with more severe cognitive impairment in Parkinson disease. Parkinsonism Relat. Disord. 34, 15–19.
Roy, A., et al., 2006. Up-regulation of microglial CD11b expression by nitric oxide. J. Biol. Chem. 281, 14971–14980.
Sandberg, M.K., et al., 2014. Prion neuropathology follows the accumulation of alternate prion protein isoforms after infective titre has peaked. Nat. Commun. 5, 4347.
Sargent, D., et al., 2017. Prion-like'propagation of the synucleinopathy of M83 transgenic mice depends on the mouse genotype and type of inoculum. J. Neurochem. 143, 126–135.
Schapansky, J., et al., 2015. The complex relationships between microglia, alpha-synuclein, and LRRK2 in Parkinson's disease. Neuroscience 302, 74–88.

Sekiyama, K., et al., 2012. Neuroinflammation in Parkinson's disease and related disorders: a lesson from genetically manipulated mouse models of-synucleinopathies. Parkinson's Dis. 2012.
Smith, W.W., et al., 2005. α-Synuclein phosphorylation enhances eosinophilic cytoplasmic inclusion formation in SH-SY5Y cells. J. Neurosci. 25, 5544–5552.
Taleb, A., et al., 2006. Raman microscopy for the chemometric analysis of tumor cells. J. Phys. Chem. B 110, 19625–19631.
Walker, D.G., Lue, L.F., 2015. Immune phenotypes of microglia in human neurodegenerative disease: challenges to detecting microglial polarization in human brains. Alzheimers Res. Ther. 7, 56.
Walker, D.G., et al., 2013. Changes in properties of serine 129 phosphorylated α-synuclein with progression of Lewy-type histopathology in human brains. Exp. Neurol. 240, 190–204.
Wang, Q., et al., 2011. Exploring Raman spectroscopy for the evaluation of glaucomatous retinal changes. J. Biomed. Opt. 16, 107006.
Wang, Y., et al., 2012. Phosphorylated α-Synuclein in Parkinson's Disease. Science Translational Medicine. vol. 4 (121ra20-121ra20).
Watts, J.C., et al., 2013. Transmission of multiple system atrophy prions to transgenic mice. Proc. Natl. Acad. Sci. 110, 19555–19560.
Wills, J., et al., 2011. Tauopathic changes in the striatum of A53T α-synuclein mutant mouse model of Parkinson's disease. PLoS One 6, e17953.
Woerman, A.L., et al., 2015. Propagation of prions causing synucleinopathies in cultured cells. Proc. Natl. Acad. Sci. 112, E4949–E4958.
Woerman, A.L., et al., 2016. Tau prions from Alzheimer's disease and chronic traumatic encephalopathy patients propagate in cultured cells. Proc. Natl. Acad. Sci. 113, E8187–E8196.
Woerman, A.L., et al., 2017. α-Synuclein: Multiple System Atrophy Prions.